

# Northumbria Research Link

Citation: Tiwari, Devendra and Fermin, David J (2017) Textured Pbl2 photocathodes obtained by gas phase anion replacement. *Electrochimica Acta*, 254. pp. 223-229. ISSN 0013-4686

Published by: Elsevier

URL: <https://doi.org/10.1016/j.electacta.2017.09.110>  
<<https://doi.org/10.1016/j.electacta.2017.09.110>>

This version was downloaded from Northumbria Research Link:  
<http://nrl.northumbria.ac.uk/id/eprint/49171/>

Northumbria University has developed Northumbria Research Link (NRL) to enable users to access the University's research output. Copyright © and moral rights for items on NRL are retained by the individual author(s) and/or other copyright owners. Single copies of full items can be reproduced, displayed or performed, and given to third parties in any format or medium for personal research or study, educational, or not-for-profit purposes without prior permission or charge, provided the authors, title and full bibliographic details are given, as well as a hyperlink and/or URL to the original metadata page. The content must not be changed in any way. Full items must not be sold commercially in any format or medium without formal permission of the copyright holder. The full policy is available online: <http://nrl.northumbria.ac.uk/policies.html>

This document may differ from the final, published version of the research and has been made available online in accordance with publisher policies. To read and/or cite from the published version of the research, please visit the publisher's website (a subscription may be required.)



## Research Paper

Textured  $\text{PbI}_2$  photocathodes obtained by gas phase anion replacement

Devendra Tiwari, David J Fermin\*

School of Chemistry, University of Bristol, Cantock's Close, Bristol BS8 1TS, United Kingdom

## ARTICLE INFO

## Article history:

Received 7 June 2017

Received in revised form 4 August 2017

Accepted 18 September 2017

Available online 23 September 2017

## Keywords:

 $\text{PbI}_2$ 

thin films

solution processing

photocathodes

hydrogen evolution

## ABSTRACT

High quality  $\text{PbI}_2$  films are prepared by a new route based on iodination of solution processed  $\text{PbS}$  films at room temperature. The  $\text{PbI}_2$  films are characterized by a highly textured morphology with flake-like particles sizing 500 and 800 nm across. Quantitative X-ray diffraction and resonance Raman spectroscopy demonstrate the crystallization of highly phase pure  $2\text{H-PbI}_2$  with lattice parameters:  $a = 4.5505(9) \text{ \AA}$ ,  $c = 6.9784(14) \text{ \AA}$ . Electronic structures and vibrational modes are calculated employing DFT. Transmittance and reflectance measurements are characterized by a sharp absorption edge corresponding to a direct band gap transition of 2.41 eV. Photoelectrochemical measurements carried out in 0.1 M KI solution showed that the material behaves as a p-type semiconductor with an apparent donor concentration of the order of  $10^{15} \text{ cm}^{-3}$  as well as stable photoresponses associated with hydrogen evolution with nearly 50% incident photon-to-current efficiency. Quantitative analysis of the spectral and potential dependence of the photocurrent responses shows that surface recombination is negligible even at the flat band potential. We conclude that  $\text{I}^-$  species stabilizes the semiconductor surface, generating an ideal semiconductor/electrolyte junction, while enabling the transfer of minority carrier from the conduction band edge dominated by lead antibonding p-orbitals

© 2017 The Authors. Published by Elsevier Ltd. This is an open access article under the CC BY license (<http://creativecommons.org/licenses/by/4.0/>).

## 1. Introduction

Lead iodide ( $\text{PbI}_2$ ) currently occupies a highly prominent role in the field of photovoltaics as a key precursor in the generation of organo-lead halide absorber layers [1,2]. These materials are characterized by high light capture-cross sections, remarkably long carrier life-times and high collection efficiencies, yielding power conversion efficiencies values as high as 22% [3,4]. A variety of protocols have been reported for the conversion of  $\text{PbI}_2$  into perovskites such as methyl-ammonium lead iodide leading to a variety of microstructures [5–12]. A fundamental issue that remains unresolved is the role of unconverted  $\text{PbI}_2$  in the performance of these devices [13–16]. In this regard, there are no reports about key properties of  $\text{PbI}_2$  as photoelectrode, including carrier diffusion length, band edge positions and dynamics of interfacial recombination [17,18].

$\text{PbI}_2$  is characterized by a band gap in the range of 2.3 to 2.6 eV and a “pseudo” 2D structure resembling that of  $\text{CdI}_2$  [19,20]. Each  $\text{PbI}_2$  slab consists of a Pb layer embedded between two I layers, where the Pb is coordinated to six I atoms forming nearly an octahedron while I is bonded to three Pb atoms in trigonal pyramid

geometry. Each of these  $\text{PbI}_2$  slabs interact weakly with neighboring slabs giving rise to different stacking patterns, leading to various polytypes which have been investigated in single crystals mainly by Raman and photoluminescence spectroscopy [21–26]. The preparation of  $\text{PbI}_2$  single crystals has been reported by a variety of approaches, including Bridgman based methods, vapor assisted growth, the hot wall technique or gel-assisted methods [19,27–31]. Polycrystalline thin films are commonly deposited by vacuum evaporation of  $\text{PbI}_2$  powders or spin/spray coating of dissolved  $\text{PbI}_2$  particles [20,32–34]. Towards the preparation of organo-halide Pb perovskites,  $\text{PbI}_2$  films are conventionally deposited by spin/or spray coating from DMF solutions. However, there are two main disadvantages of this route: (i) film conformity over large area is difficult to achieve due to the low solubility of  $\text{PbI}_2$ , and (ii) films tends to be highly compact, requiring prolong exposures at elevated temperature to allow complete diffusion of the organic ligand [16,31,35–37].

In this article, we describe an entirely new approach for depositing phase pure  $\text{PbI}_2$  films displaying high quality optoelectronic properties. The two-step method consists of solution processing of a  $\text{PbS}$  thin films followed by gas phase iodination at 200 °C. The structure and optical properties of the films were investigated by, X-ray Diffraction (XRD), Scanning Electron Microscopy (SEM), Raman spectroscopy, diffuse reflectance and room temperature photoluminescence. Experimental analysis,

\* Corresponding author.

E-mail address: [david.fermin@bristol.ac.uk](mailto:david.fermin@bristol.ac.uk) (D.J. Fermin).

supported by ab-initio Density Function Theory (DFT) calculations, clearly demonstrated the generation of the 2H- form of  $\text{PbI}_2$  with a high degree of phase purity. For the first time, we show that  $\text{PbI}_2$  can act as a stable photocathode for hydrogen generation exhibiting negligible surface recombination even at the flat band potential. We conclude that  $\text{I}^-$  in solution stabilizes the surface of  $\text{PbI}_2$ , suppressing photodecomposition and enabling the transfer of minority carriers via the Pb antibonding p-orbitals.

## 2. Experimental

### 2.1. $\text{PbI}_2$ synthesis

$\text{PbI}_2$  thin films are deposited by an anion replacement technique, involving iodination of PbS films. PbS is deposited on F-doped  $\text{SnO}_2$  (FTO, Aldrich) by spin-coating a metal-organic precursor solution containing lead acetate (6 M) and thiourea (6 M) dissolved in acetic acid. Spin-coating is carried out at 2000 rpm for 30 seconds, followed by thermolysis at 200 °C in air for 5 mins, resulting in about 450 nm thick film. The PbS films are exposed to 100 mg of  $\text{I}_2$  a closed lid petri dish heated to 200 °C for 10 min. PbS conversion to  $\text{PbI}_2$  is clearly visible within minutes. The  $\text{PbI}_2$  films are removed from the iodination petri-dish, and subsequently rinsed with ultrapure water and methanol in order to wash any superficial  $\text{I}_2$  or other by-products, followed by drying with high purity Argon.

### 2.2. Instrumentation

Structural analysis was carried out using powder X-ray diffraction (Bruker D8 Advance), with quantitative Rietveld structure refinement employing the Fullprof software suite. Pseudo-Voigt functions were used as fitting functions. Raman spectra were recorded at room temperature using a 514 nm laser excitation (Renishaw, inVia). Film morphology was imaged with a scanning electron microscopy (Jeol iT300) at 20 kV with secondary electron detector (films were coated with a 15 nm layer of C). The elemental composition of films is measured using Oxford x-max 80 mm<sup>2</sup> Energy Dispersive Analysis of X-rays, EDAX detector coupled to the SEM. Transmittance and reflectance spectroscopy of films is performed using a UV-vis spectrometer (Shimadzu 2600). Photoluminescence spectrum is measured at 80 K with 514 nm laser excitation source (Renishaw, inVia). Electrochemical measurements were performed under potentiostatic conditions (Ivium compactstat) in 0.1 M KI Ar-purged aqueous solution, with a Pt wire counter-electrode and Ag/AgCl reference electrode. External quantum efficiency measurements were acquired under chopped illumination and lock-in detection (SRS 830), with a Bentham halogen lamp and a monochromator (Bentham TMC300) in wavelength range of 400 to 600 nm. Interfacial capacitance was measured with a Solartron Modulab impedance analyzer.

### 2.3. DFT calculations

Ab-initio DFT calculation on  $\text{PbI}_2$  are done with CASTEP suite. All the calculations are performed using a PBESOL functional, with norm conserving pseudopotentials and a Monkhorst – Pack k point mesh of  $11 \times 11 \times 8$ . It must be mentioned here that although the norm conserving pseudopotentials for Pb does account for relativistic effects but remaining non-relativistic effect responsible for spin-orbital coupling is beyond plane-wave code employing norm conserving pseudopotentials thus spin-orbit spitting at band edges are disregarded. For geometry optimization the energy cut off and convergence window is set to 910 eV and  $1 \times 10^{-6}$  eV, respectively. The structure is relaxed until forces acting on atoms are converged below  $1 \times 10^{-5}$  eV/Å. For Band structure and density

of states calculation, the convergence window is restricted to  $1 \times 10^{-5}$  eV with 0.07 1/Å spacing. Density functional perturbation theory based on linear response formalism under PBESOL is employed for the calculations of polarizability and Raman spectrum. For optical properties, imaginary dielectric function ( $\epsilon_i$ ) is numerically evaluated from the wavefunctions of occupied and unoccupied electronic states. Real dielectric function ( $\epsilon_r$ ) is calculated from the Kramer-Kronig transformation of  $\epsilon_i$ . Using dielectric function, first refractive indices are obtained from which absorption and reflectivity spectra are computed.

## 3. Results and discussion

Fig. 1a shows a characteristic X-ray diffractogram of a  $\text{PbI}_2$  films along with quantitative structure refinement fits using Rietveld analysis. The diffractogram is consistent with a highly polycrystalline form. The quantitative structure refinement shows an excellent fit to the  $\text{PbI}_2$  phase, with profile and weighted profile correlation fit parameters:  $R_p$  and  $R_{wp}$  of 2.22 and 3.01%, respectively. The analysis confirms a highly phase pure trigonal  $\text{PbI}_2$  with the space group P-32/m1 as illustrated in the inset of Fig. 1a. This space group is characterised by a  $D_{3d}$  point group symmetry, which is consistent with 2H- polytype of  $\text{PbI}_2$ . XRD analysis showed that the lattice parameters for the  $\text{PbI}_2$  unit cell correspond to  $a = 4.55054 \pm 0.00093$  Å and  $c = 6.97847 \pm 0.00142$  Å. The site coordination of Pb and I atom along with their occupancies resulting from the structure refinement can be found in the

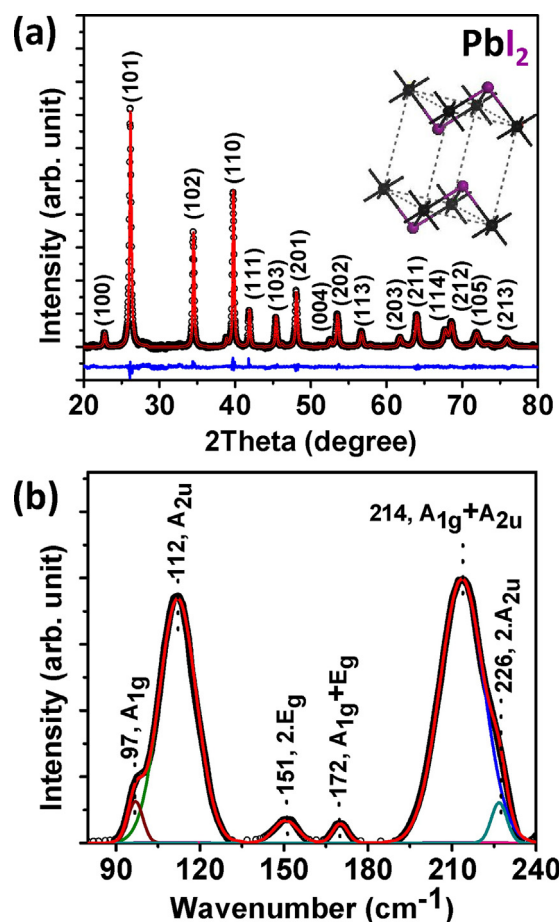


Fig. 1. X-ray diffractogram and quantitative structure refinement of the as grown  $\text{PbI}_2$  film (a). The inset showed the trigonal  $\text{PbI}_2$  unit cell with the space group P-32/m1 used in the structure refinement. Room temperature Raman spectrum obtained upon excitation at 514 nm, with assignment of observed vibrational modes (b).

supplementary Information (Table s1). In accordance with previous structural studies [38], we observed that each Pb atom is in proximity to three I atoms forming a trigonal pyramid shape, where I is located at the summit, the Pb-I distance is 3.2091(10) Å and the angle centred at Pb-I-Pb is 90.31(6)°. Each Pb is coordinated to 6 I atoms (octahedral coordination). Each of unit cell includes two of such of pyramids facing each other by the apex I atom lying at body diagonal of cell and distance between them being 4.2125(18) Å, isolating each PbI<sub>2</sub> slab. A schematic of the unit cell is depicted as inset to Fig. 1. EDAX measurements showed a Pb/I elementary ratio of 32.1%/67.9%, corresponding to a slight I excess.

Fig. 1b illustrates a room temperature Raman spectrum of the PbI<sub>2</sub> film obtained with excitation at 514 nm. Considering a 2H-polytype, 9 degrees of freedom and corresponding normal modes can be expected via the following irreducible representation:  $\Gamma_{\text{optic}} = A_{1g} + E_g + A_{2u} + E_u$  and  $\Gamma_{\text{acoustic}} = A_{2u} + E_u$ . The Raman active  $A_{1g}$  and  $E_g$  modes involve symmetric stretching and shearing of two iodine atoms, respectively. On the other hand, the  $A_{2u}$  and  $E_u$  modes occur in the far IR region, involving the vibration of the Pb layer against the I layer either in perpendicular ( $A_{2u}$ ) or in parallel ( $E_u$ ) to the basal plane. For the sake of clarity, animations of the key Raman modes are presented in the SI. Raman spectrum calculated by density functional perturbation theory (DFPT), (Figure s1) shows two bands due to  $E_g$  and  $A_{1g}$  modes at 81 and 97 cm<sup>-1</sup>, respectively, consistent with literature values of about 76 and 97 cm<sup>-1</sup> [22]. In addition to the main Raman mode, the spectrum in Fig. 1b features peaks at 112, 151, 172, 214 and 226 cm<sup>-1</sup>. These peaks are associated with forbidden modes enabled by resonant Raman Effect. As the excitation energy is closed to the band gap energy, forbidden and allowed modes can be coupled through higher order terms, resulting in the appearance of  $A_{2u}$  (LO) mode at 112 cm<sup>-1</sup>. Stronger LO mode responses with respect to the active  $A_{1g}$  mode has been observed when the c-plane of the PbI<sub>2</sub> flakes (or crystals) is oriented antiparallel to the incident excitation [39]. As shown below, this appears to be consistent with film morphology. The other peaks can be assigned to either higher order or combination modes (Fig. 1b), while the absence of Davydov splitting suggests that no 4H-PbI<sub>2</sub> polytype is present in detectable amounts [22]. Consequently, X-ray diffraction and Raman spectroscopy provides conclusive evidence that the gas phase anion replacement method leads to phase pure 2H-PbI<sub>2</sub>.

The band structure shown in Fig. 2 is obtained by ab-initio DFT plane wave calculations and PBESOL functionals. Geometry optimization yielded a Pb-I bond distance and Pb-I-Pb bond angle of 3.1739 Å and 91.13°, respectively, with lattice constants of  $a = 4.5326$  Å and  $c = 6.9863$  Å. The calculated structure parameters are within 1% of the experimental values obtained from the XRD measurements. The conduction band minimum (CBM) and valence band maximum (VBM) lie at special point A, with a direct band gap of 2.052 eV. The band gap value is somewhat underestimated, which is a consequence of using GGA functional. The absorption and reflectivity spectra computed from these calculations are shown in the supplementary Information (Figure s2). Flat regions at the top of valence band are confined to an energy range of 0.87 eV, which is consistent with rather localized orbitals. On the other hand, the conduction band disperses over a range of 2.21 eV due to hybridised nature of the orbitals.

The total density of states along with the partial density of states of participating Pb and I atoms are shown in Fig. 2b. Strongly localised bands at around -16, -11 and -8 eV are linked to Pb 5d, I s and Pb s orbitals, respectively. Pb and I s orbitals also generate bands above the bottom of the conduction band. The major contribution to the VBM arises from I 5p<sub>z</sub> orbitals, with small contributions from Pb 6s and 6p<sub>z</sub> orbitals, while the two bands below the VB composed of 6p<sub>x</sub> and 6p<sub>y</sub> exclusively. The CBM minimum is composed of the antibonding orbitals with 2/3

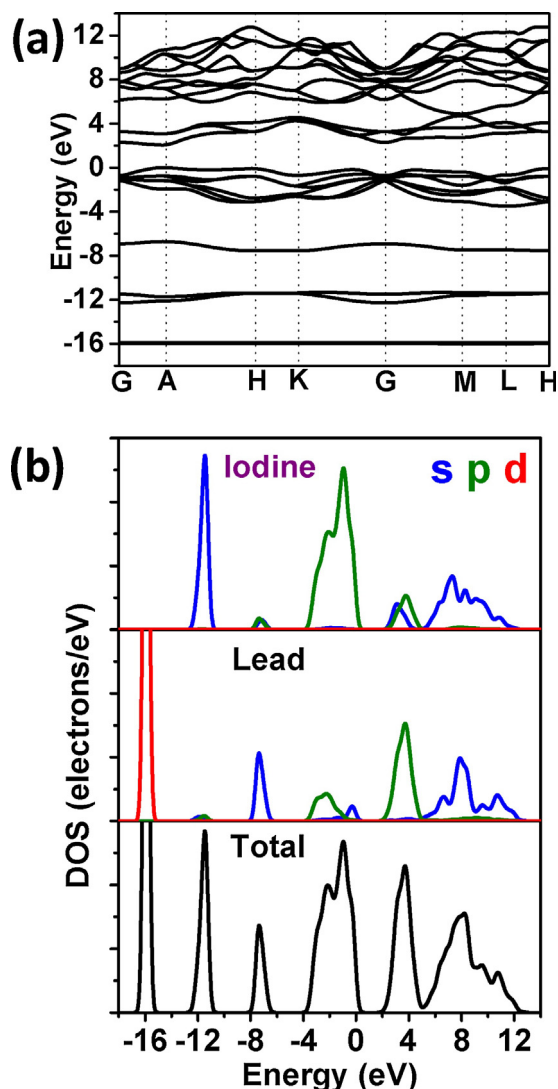
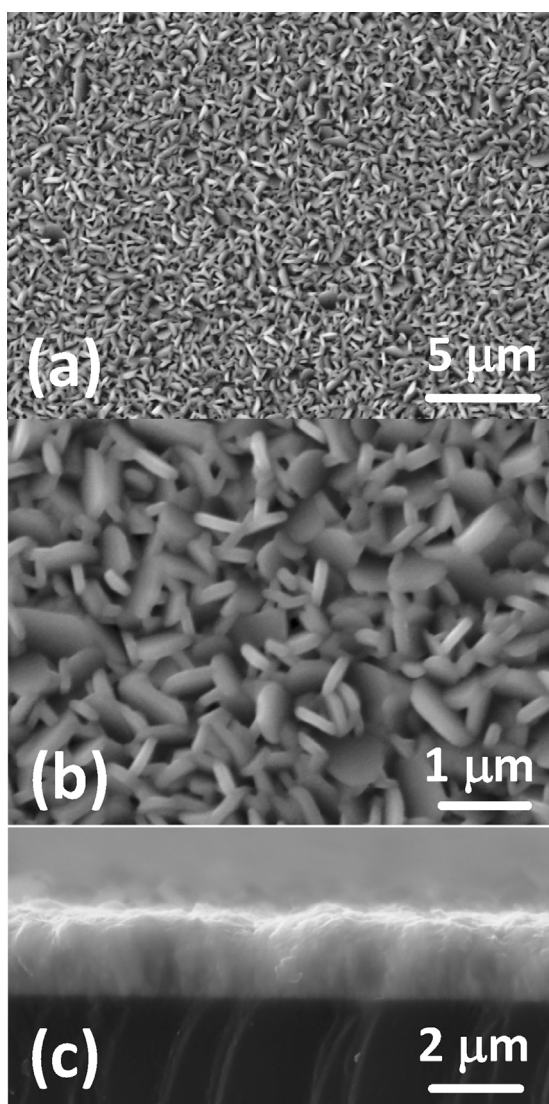


Fig. 2. Band structure (a) and density of states (b) calculated for PbI<sub>2</sub> using the ab-initio DFT with PBESOL functional.

participation of Pb 6p<sub>z</sub> and 1/3 from I s and 5p<sub>z</sub> orbitals. It should be mentioned that the expected splitting of the Pb p orbital is not observed due to the fact that spin-orbital coupling are excluded from the Hamiltonian.

Fig. 3a displays a characteristic SEM image of PbI<sub>2</sub> films obtained by the gas phase anion replacement method, exhibiting a remarkable homogeneity over several tens of micrometers. A closer examination (Fig. 3b) shows individual PbI<sub>2</sub> crystallites with the c-plane predominantly oriented antiparallel to the substrate plane. The particle sizes range from 500 to 800 nm across and 200 to 300 nm thick, while the quasi-2D structure of the grains is inherent to PbI<sub>2</sub> [27,32,40]. The cross-sectional image in Fig. 3c further demonstrates the highly compact nature of the film, with a thickness of 1.8 μm. In addition to the film surface homogeneity, this method also provides fine control over film thickness by adjusting the amount of PbS molecular precursor spin coated at the substrate.

The transmittance and reflectance spectra of a PbI<sub>2</sub> film are shown in Fig. 4a, revealing a sharp transition with an onset at 2.45 eV. This transition corresponds to fundamental band-to-band excitation. The absorption coefficient ( $\alpha$ ) calculated from the optical data is of the order of 10<sup>4</sup> cm<sup>-1</sup> for wavelengths below 2.41 eV and is in agreement with calculated spectrum (Figure s2).



**Fig. 3.** SEM micrograph of  $\text{PbI}_2$  film: Top view at different magnifications illustrating a homogenous topography composed of flake-like structures stacked out-of-plane, with sizes from 500 to 800 nm across and 200 to 300 nm thick (a, b). Cross-section view, revealing the compact nature of the film with thickness 1.8  $\mu\text{m}$  (c).

The inset in Fig. 4a shows the Tauc plot revealing an optical band gap of 2.41 eV, which is consistent with previous studies [41]. The photoluminescence spectrum of  $\text{PbI}_2$  films at 80 K is displayed in Fig. 4b, showing a number of sharp features near the absorption edge (region I) and a broad band below 1.8 eV (region II). The peak at 2.1 eV, commonly referred to as the G-band, is attributed to excited  $\text{Pb}^+$  or  $\text{Pb}^{2+}$  centres [42,43]. The peaks in the region 2.33–2.36 eV (D-band) are prominent features in cases where excitation and emission collection take place off the  $\text{PbI}_2$  c-plane, suggesting that these responses are associated with stacking faults (although surface  $\text{Pb}^+$  states have also been postulated) [39,43,44]. The broad peak in region II may be linked to bulk sub-band gap states.

Fig. 5a displays the interfacial capacitance at the  $\text{PbI}_2$ /electrolyte junction, containing 0.1 M KI, as function of the electrode potential. The capacitance was calculated from impedance responses at 2 kHz. Only a small variation of the capacitance was observed over a wide range of frequencies. The Mott-Schottky plot shown in Fig. 5b exhibit a linear behaviour over a large

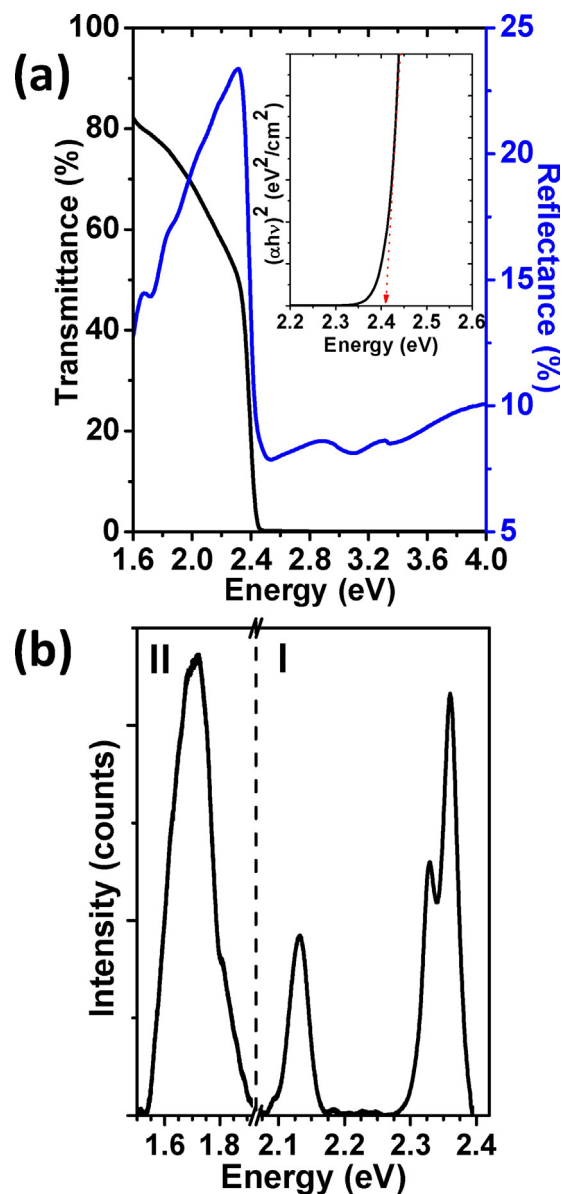


**Fig. 4.** Transmittance and reflectance spectra of a 1  $\mu\text{m}$   $\text{PbI}_2$  film, with the inset showing the corresponding Tauc plot revealing a band gap of 2.41 eV (a). Photoluminescence spectrum of  $\text{PbI}_2$  films measured at 80 K (b).

potential range until the flat-band value ( $E_{fb}$ ). This behaviour is consistent with an ideal semiconductor/electrolyte junction operating under band edge pinning conditions. The Mott-Schottky equation (1) relates the capacitance at the space charge layer with the corresponding potential drop ( $E_{fb} - E$ ):

$$\frac{1}{C^2} = \frac{2}{A^2 q \epsilon \epsilon_0 N_A} \left[ (E_{FB} - E) - \frac{kT}{q} \right] \quad (1)$$

where,  $N_A$  is the number of acceptor states (doping density),  $A$  is the surface area and  $\epsilon$  is the relative permittivity of  $\text{PbI}_2$  (taken as 7.5) [41]. The slope of Mott-Schottky plot is consistent with a p-type semiconductor with an effective  $N_A = 1.6 \times 10^{15} \text{ cm}^{-3}$ . The relatively small value of  $N_A$  is consistent with the low dark conductivity commonly observed in these materials [45]. It should also be mentioned that our analysis may overestimate the value of  $N_A$  given that the capacitance is normalized by the geometric

surface area of the electrode. The value of  $E_{fb}$  extrapolated from the Mott-Schottky plot corresponds to 0.175 V vs Ag/AgCl. As far as we are aware of, this is the first estimation reported of the flat-band potential of  $PbI_2$  electrodes.

Fig. 6a shows photocurrent transients as a function of the photon flux (516 nm) at  $-0.4$  V. The negative photocurrent implies p-type conductivity in agreement with the Mott-Schottky analysis. The linear dependence of photocurrent on photon flux as well as the sharp onset and decay in-phase with the trigger square light pulse strongly suggests the absence of surface recombination at this potential. Even more remarkable is the weak potential dependence of the photocurrent transient shown in the linear sweep voltammogram display in Fig. 6b. The photocurrent magnitude increases as the potential is swept towards negative values, with a sizeable value at the flat band potential. High concentrations of  $I^-$  in the electrolyte solution at neutral pH was found crucial for the stability of the  $PbI_2$  in the dark and under illumination.

The photocurrent action spectra of the  $PbI_2$  films recorded at  $-0.5$  V vs Ag/AgCl in Ar-saturated 0.1 M KI is displayed in Fig. 7a. The photocurrent magnitude were recorded under chopped illumination and lock-in detection (27 Hz) and normalised by the photon flux measured by a calibrated Si photodiode, including reflection losses estimated from the reflectance spectra (Fig. 4a). The quantum efficiency (QE) shows an onset at 2.35 eV, followed by a step increase to 50%. The first derivative of the EQE plot near the onset shows a narrow peak located at 2.42 eV (data not shown), which is fully consistent with the optical band gap obtained from

the Tauc plot (Fig. 4a). No sub-band gap photoresponses were observed in our films. Fig. 7b displays the dependence of the QE at 2.5 eV on the applied potential employing chopped illumination and lock-in detection (27 Hz). In agreement with Fig. 6b, the photocurrent magnitude show a slight increase as the potential is negatively swept. Fig. S3 shows the real and imaginary component of the photocurrent for three different electrodes. These trends clearly show that the photocurrent essentially remains in-phase at the flat band potential, confirming the absence of recombination losses. The figure also illustrates the reproducibility of the film properties, with dispersion of the photocurrent responses below 5%.

In the absence of  $O_2$ , cathodic photocurrents can originate from only two processes: (1) photo decomposition of  $PbI_2$  leading to  $I^-$  in solution and Pb metallization or (2) the hydrogen evolution reaction. We have operated the photoelectrodes for over 180 minutes across a wide potential range below 0.17 V without any significant loss of photoactivity, strongly suggesting that cathodic photocorrosion is negligible. It could also be argued that traces of  $I_2$  and/or  $I_3^-$  could be present in the electrolyte solution which may act as electron acceptor. However, this is not consistent with the fact that photoresponses are not limited by diffusion of electron acceptors in solution. Indeed, photocurrent responses remain in-phase and linearly dependent with the photon-flux for values above  $10 \mu A$ , indicating that hydrogen evolution is the primary redox processes under illumination.

The spectral and potential dependence of the QE can be described, as a first approximation, in terms of the Gartner

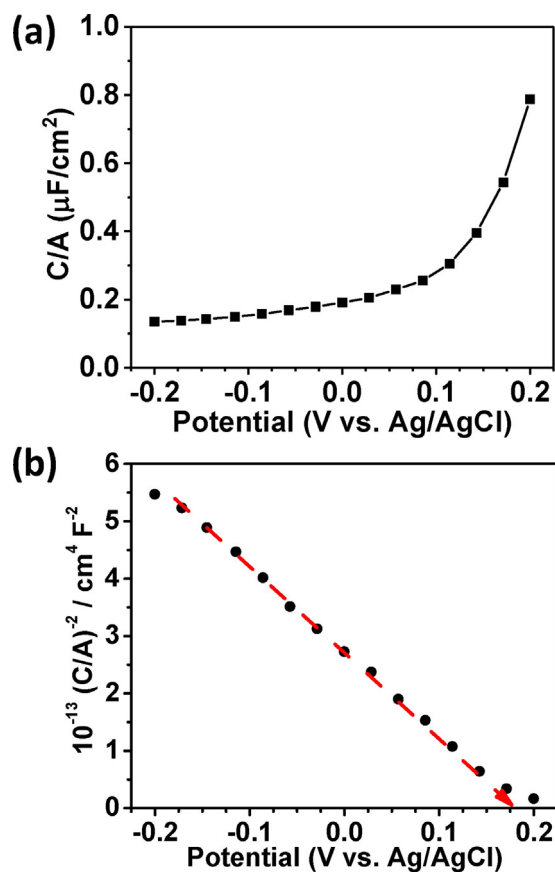


Fig. 5. Potential dependence of interfacial capacitance of  $PbI_2$  electrode measured at 2 kHz in Ar-saturated 0.1 M KI (a). Mott-Schottky plot derived using the capacitance data (b). The flat band potential ( $E_{fb}$ ) estimated from the analysis corresponds to 0.175 V vs Ag/AgCl.

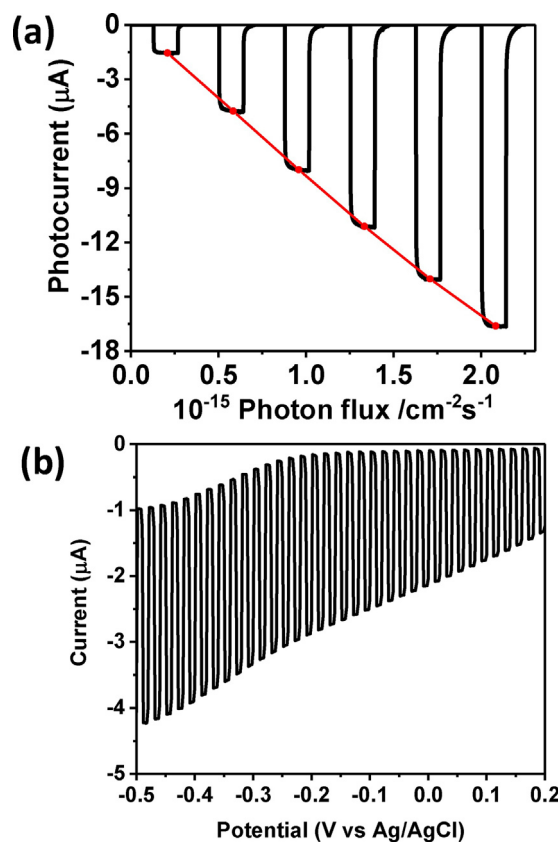
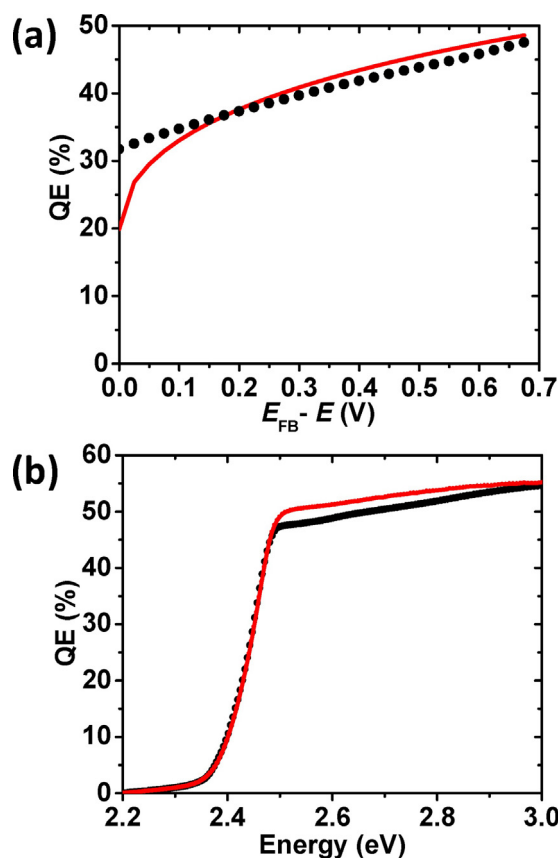


Fig. 6. Transient Photocurrent of  $PbI_2$  film as a function of photon flux (516 nm) at  $-0.4$  V vs. Ag/AgCl in 0.1 M Ar saturated aqueous KI solution (a) and linear sweep voltammogram under square pulsed illumination (516 nm LED) (b).



**Fig. 7.** Quantum efficiency (QE) of  $\text{PbI}_2$  film at  $-0.5$  V vs. Ag/AgCl as a function of excitation energy in the same electrolyte solution (a). Potential dependence of QE measured at  $2.5$  eV and photon flux  $\Phi_{\text{photon}} = 2.15 \times 10^{14} \text{ cm}^{-2} \text{ s}^{-1}$  (b). The continuous red line in (a) and (b) corresponds to a simulation based on the Gartner model assuming a minority carrier diffusion length of  $80$  nm.

expression [46,47],

$$QE = 1 - \frac{\exp(-\alpha w)}{1 + \alpha L_n} \quad (2)$$

where  $L_n$  is the carrier diffusion length and  $w$  is the width of the space charge region, given by:

$$w = \sqrt{\frac{2\epsilon\epsilon_0(E_{FB} - E)}{qN_A}} \quad (3)$$

Using the absorption coefficient ( $\alpha$ ) estimated from the optical data (Fig. 4a) and the apparent  $N_A$  obtained from the impedance data, simulations of the QE responses (red lines in Fig. 7a and b) resulted in  $L_n$  of the order of  $80$  nm. The small differences observed between experimental and simulated QE values in Fig. 7b are mainly linked to other reflection losses not considered in the analysis (e.g. air/cell window and cell window/electrolyte boundary). The light penetration depth calculated from the absorption coefficient at the band edge is approximately  $280$  nm, which is larger than the characteristic carrier retrieval distance given by  $L_n + w \approx 200$  nm [48]. This analysis strongly suggests that the QE is mainly determined by bulk recombination processes.

A striking proximity between experimental and modelled potential dependent QE is also observed in Fig. 7b. There is a slight discrepancy at potentials very close to  $E_{fb}$  which may result from uncertainties in the  $N_A$  value or a degree of Fermi level pinning. This is not entirely surprising given the surface texture of the  $\text{PbI}_2$  films. However, our analysis does confirm that surface recombination

losses are insignificant even at the  $E_{fb}$ . Such behaviour has only been observed on semiconductor single crystals in the presence of fast minority carrier scavengers, which may also promote surface stabilisation [49]. We propose that the stabilisation introduced by  $\text{I}^-$  in solution enables minority carriers mainly localised at the antibonding Pb p-orbitals to be captured by water, promoting hydrogen evolution rather than Pb metallisation. It should be mentioned that the conduction band edge is more negative than  $-2.2$  V vs Ag/AgCl ( $-1.59$  V vs RHE), providing a large driving force for hydrogen evolution. Indeed, the ideal behaviour of the semiconductor/electrolyte junction indicates that the quasi-Fermi level of electrons is effectively determined by the conduction band edge. Such outstanding photoactivity towards the hydrogen evolution reaction at neutral pH, in the absence of co-catalyst, is rather unexpected from polycrystalline semiconductor thin-film. The low recombination rate could also be linked to the splitting of the conduction band edge at the  $\Gamma$  point as a result of spin-orbit coupling introduced by lead orbitals [50,51]. The so-called ‘‘Rashba splitting’’ is widely considered as the key phenomenon behind the long carrier life-time in organo-lead halide perovskites [52].

#### 4. Conclusions

A new method for generating high quality  $\text{PbI}_2$  films is described based on solution processing of PbS followed by gas phase iodisation at  $200^\circ\text{C}$ . The films are compact, exhibiting flake like crystallites with sizes in the range of  $500$  to  $800$  nm. Quantitative XRD and Raman analysis, supported by DFT calculations demonstrated the formation of the 2H- form of  $\text{PbI}_2$  with a very high degree of phase purity. Diffuse reflectance/transmittance and photoluminescence spectroscopy are consistent with a direct band-gap transition and  $2.41$  eV. Photoelectrochemical studies in KI containing solution show characteristic responses of p-type electrodes with an effective acceptor density of the order or  $10^{15} \text{ cm}^{-3}$ . Quantitative analysis of the potential and spectral responses of the photocurrent responses demonstrates that the  $\text{I}^-$  species stabilises the semiconductor surface, while no evidence of surface recombination are seen even at the flat band potential. The photocurrent responses are stable over time allowing to conclude that hydrogen evolution reaction is essentially determined by the flux of minority carriers to the thin-film surface. The absence of surface recombination in this material may also point towards a fundamental aspect of Pb based absorbers which could be linked to the outstanding properties of organo-halide Pb perovskite systems. Indeed, the structure and topography of these  $\text{PbI}_2$  films may provide an ideal platform for generating high quality  $\text{CH}_3\text{NH}_3\text{PbI}_3$  absorbers.

#### Supporting Information

Structural parameters obtained from XRD refinement, theoretical Raman spectrum of  $\text{PbI}_2$  calculated from density functional perturbation, absorption and reflectivity spectra plotted for fully isotropic polarization (PDF).

Videos describing the Raman vibrational modes  $A_{1g}$ ,  $A_{2u}$ ,  $E_g$  and  $E_u$ .

#### Acknowledgements

DT and DJF are indebted to UK Engineering and Physical Sciences Research Council (EPSRC) the PVTEAM grant (EP/L017792/1). DJF also acknowledges the support by the Institute of Advanced Studies of the University of Bristol, (University Research Fellowship 2015). Electron microscopy and impedance analysis were acquired with instrumentation supported by EPSRC Capital grant (EP/K035746/1). DFT calculations were performed at the Advanced Computing Research Centre, University of Bristol ([www.bris.ac.uk/acrc/](http://www.bris.ac.uk/acrc/)).

## Appendix A. Supplementary data

Supplementary data associated with this article can be found, in the online version, at <http://dx.doi.org/10.1016/j.electacta.2017.09.110>.

## References

- [1] Y. Yang, J. You, Make perovskite solar cells stable, *Nature* 544 (2017) 155.
- [2] M.D. McGehee, Perovskite solar cells: Continuing to soar, *Nat. Mater* 13 (2014) 845.
- [3] S.S. Shin, E.J. Yeom, W.S. Yang, S. Hur, M.G. Kim, J. Im, J. Seo, J.H. Noh, S. Il Seok, Colloidally prepared La-doped BaSnO<sub>3</sub> electrodes for efficient, photostable perovskite solar cells, *Science* 356 (2017) 167.
- [4] M. Saliba, T. Matsui, K. Domanski, J.-Y. Seo, A. Ummadisingu, S.M. Zakeeruddin, J.-P. Correa-Baena, W.R. Tress, A. Abate, A. Hagfeldt, M. Gratzel, Incorporation of rubidium cations into perovskite solar cells improves photovoltaic performance, *Science* 354 (2016) 206.
- [5] Y. Jo, K.S. Oh, M. Kim, K.H. Kim, H. Lee, C.W. Lee, D.S. Kim, High Performance of Planar Perovskite Solar Cells Produced from Pbl<sub>2</sub>(DMSO) and Pbl<sub>2</sub>(NMP) Complexes by Intramolecular Exchange, *Adv. Mater. Interfaces* 3 (2016) 1500768.
- [6] T. Liu, Q. Hu, J. Wu, K. Chen, L. Zhao, F. Liu, C. Wang, H. Lu, S. Jia, T. Russell, R. Zhu, Q. Gong, Mesoporous Pbl<sub>2</sub> Scaffold for High-Performance Planar Heterojunction Perovskite Solar Cells, *Adv. Energy Mater.* 6 (2016) 1501890.
- [7] A. Sharenko, M.F. Toney, Relationships between Lead Halide Perovskite Thin-Film Fabrication Morphology, and Performance in Solar Cells, *J. Am. Chem. Soc.* 138 (2016) 463.
- [8] W. Li, J. Fan, J. Li, Y. Mai, L. Wang, Controllable grain morphology of perovskite absorber film by molecular self-assembly toward efficient solar cell exceeding 17%, *J. Am. Chem. Soc.* 137 (2015) 10399.
- [9] Y. Wu, A. Islam, X. Yang, C. Qin, J. Liu, K. Zhang, W. Peng, L. Han, Retarding the crystallization of Pbl<sub>2</sub> for highly reproducible planar-structured perovskite solar cells via sequential deposition, *Energy Environ. Sci.* 7 (2014) 2934.
- [10] D. Bi, A.M. El-Zohry, A. Hagfeldt, G. Boschloo, Improved Morphology Control Using a Modified Two-Step Method for Efficient Perovskite Solar Cells, *ACS Appl. Mater. Interfaces* 6 (2014) 18751.
- [11] J.H. Im, H.S. Kim, N.G. Park, Morphology-photovoltaic property correlation in perovskite solar cells: One-step versus two-step deposition of CH<sub>3</sub>NH<sub>3</sub>PbI<sub>3</sub>, *APL Mater.* 2 (2014) 81510.
- [12] E. Zheng, X.F. Wang, J. Song, L. Yan, W. Tian, T. Miyasaka, Pbl<sub>2</sub>-Based Dipping-Controlled Material Conversion for Compact Layer Free Perovskite Solar Cells, *ACS Appl. Mater. Interfaces* 7 (2015) 18156.
- [13] Y.C. Kim, N.J. Jeon, J.H. Noh, W.S. Yang, J. Seo, J.S. Yun, A. Ho-Baillie, S. Huang, M. A. Green, J. Seidel, T.K. Ahn, S. Il Seok, Beneficial Effects of Pbl<sub>2</sub> Incorporated in Organo-Lead Halide Perovskite Solar Cells, *Adv. Energy Mater.* 6 (2016) 1502104.
- [14] F. Liu, Q. Dong, M.K. Wong, A.B. Djuricic, A. Ng, Z. Ren, Q. Shen, C. Surya, W.K. Chan, J. Wang, A.M.C. Ng, C. Liao, H. Li, K. Shih, C. Wei, H. Su, J. Dai, Is Excess Pbl<sub>2</sub> Beneficial for Perovskite Solar Cell Performance? *Adv. Energy Mater.* 6 (2016) 1502206.
- [15] U. Kwon, M.M. Hasan, W. Yin, D. Kim, N.Y. Ha, S. Lee, T.K. Ahn, H.J. Park, Investigation into the Advantages of Pure Perovskite Film without Pbl<sub>2</sub> for High Performance Solar Cell, *Sci. Rep.* 6 (2016) 35994.
- [16] D.H. Cao, C.C. Stoumpos, C.D. Malliakas, M.J. Katz, O.K. Farha, J.T. Hupp, M.G. Kanatzidis, Remnant Pbl<sub>2</sub>, an unforeseen necessity in high-efficiency hybrid perovskite-based solar cells? *APL Mater.* 2 (2014) 091101.
- [17] C.K. Chua, Z. Sofer, C.S. Lim, M. Pumera, Inherent electrochemistry of layered post-transition metal halides: The unexpected effect of potential cycling of Pbl<sub>2</sub>, *Chem. – A Eur. J.* 21 (2015) 3073.
- [18] A.J. Nozik, M.W. Peterson, Quantum Size Effects in Layered Semiconductor Colloids, in: A. Aruchamy (Ed.), *Photoelectrochemistry and photovoltaics of layered semiconductors*, Kluwer Academic publishers, Dordrecht, The Netherlands, 1992, pp. 131.
- [19] H.K. Henisch, J. Dennis, Crystal growth in gels, *Mater. Res.* 26 (1965) 493.
- [20] T. Ghosh, S. Bandyopadhyay, K.K. Roy, S. Kar, A.K. Lahiri, A.K. Maiti, K. Goswami, Optical and structural properties of lead iodide thin films prepared by vacuum evaporation method, *Cryst. Res. Technol.* 43 (2008) 959.
- [21] P.M. Gnatenko, Y.P. Piryatinski, A.P. Bukivskii, P.A. Skubenko, R.V. Gamernyk, Time-resolved photoluminescence spectroscopy of excitons in layered semiconductor Pbl<sub>2</sub> nanoclusters, *J. Appl. Phys.* 112 (2012) 93708.
- [22] M.Y. Khilji, W.F. Sherman, G.R. Wilkinson, Raman study of three polytypes of Pbl<sub>2</sub>, *J. Raman Spectrosc.* 13 (1982) 127.
- [23] F. Lévy, a. Mercier J.-P. Voitchevsky, Band-edge photoluminescence of Pbl<sub>2</sub>, *Solid State Commun.* 15 (1974) 819.
- [24] M.P. Lisitsa, F.V. Motsnyi, O.S. Zinets, Interlayer excitons: experiments and Theory, *Ukr. J. Phys.* 48 (2003) 810.
- [25] S. Nakashima, Raman study of polytypism in vapor-grown Pbl<sub>2</sub>, *Solid State Commun.* 16 (1975) 1059.
- [26] W. Sears, M. Klein, J. Morrison, Polytypism and the vibrational properties of Pbl<sub>2</sub>, *Phys. Rev. B.* 19 (1979) 2305.
- [27] T. Hayashi, M. Kinpara, J.F. Wang, K. Mimura, M. Isshiki, Growth of Pbl<sub>2</sub> single crystals from stoichiometric and Pb excess melts, *J. Cryst. Growth.* 310 (2008) 47.
- [28] T. Hayashi, M. Kinpara, J.F. Wang, K. Mimura, M. Isshiki, Growth of ultra-high purity Pbl<sub>2</sub> single crystal: (1) Preparation of high purity Pbl<sub>2</sub>, *Cryst. Res. Technol.* 43 (2008) 9.
- [29] D.S. Bhavsar, K.B. Saraf, Morphology of Pbl<sub>2</sub> Crystals Grown by Gel Method, *Cryst. Res. Technol.* 37 (2002) 51.
- [30] X.H. Zhu, Z.R. Wei, Y.R. Jin, A.P. Xiang, Growth and characterization of a Pbl<sub>2</sub> single crystal used for gamma ray detectors, *Cryst. Res. Technol.* 42 (2007) 456.
- [31] Z. Zheng, A. Liu, S. Wang, Y. Wang, Z. Li, W.M. Lau, L. Zhang, In situ growth of epitaxial lead iodide films composed of hexagonal single crystals, *J. Mater. Chem.* 15 (2005) 4555.
- [32] M. Schieber, N. Zamoshchik, O. Khakhan, A. Zuck, Structural changes during vapor-phase deposition of polycrystalline-Pbl<sub>2</sub> films, *J. Cryst. Growth.* 310 (2008) 3168.
- [33] J.F. Condeles, R.C.Z. Lofrano, J.M. Rosolen, M. Mulato, Stoichiometry, Surface and Structural Characterization of Lead Iodide thin Films, *Brazilian J. Phys.* 36 (2006) 320.
- [34] T.K. Chaudhuri, H.N. Acharya, Preparation of lead iodide films by iodination of chemically deposited lead sulphide films, *Mater. Res. Bull.* 17 (1982) 279.
- [35] H.S. Jung, N.G. Park, Perovskite solar cells: From materials to devices, *Small* 11 (2015) 10.
- [36] F. Fu, L. Kranz, S. Yoon, J. Loekinger, T. Jaeger, J. Perrenoud, T. Feurer, C. Gretener, S. Buecheler, A.N. Tiwari, Controlled growth of Pbl<sub>2</sub> nanoplates for rapid preparation of CH<sub>3</sub>NH<sub>3</sub>PbI<sub>3</sub> in planar perovskite solar cells, *Phys. Status Solidi Appl. Mater. Sci.* 212 (2015) 2708.
- [37] C. Ying, C. Shi, N. Wu, J. Zhang, M. Wang, A two-layer structured Pbl<sub>2</sub> thin film for efficient planar perovskite solar cells, *Nanoscale.* 7 (2015) 10.
- [38] W. Palosz, polytypes 2H and 4H: a study of the 2H–4H transition, *J. Phys. Condens. Matter* 2 (1999) 5285.
- [39] I. Baltog, M. Baibarac, S. Lefrant, Quantum well effect in bulk Pbl<sub>2</sub> crystals revealed by the anisotropy of photoluminescence and Raman spectra, *J. Phys. Condens. Matter.* 21 (2009) 25507.
- [40] J. Zhang, T. Song, Z. Zhang, K. Ding, F. Huang, B. Sun, Layered ultrathin Pbl<sub>2</sub> single crystals for high sensitivity flexible photodetectors, *J. Mater. Chem. C.* 3 (2015) 4402.
- [41] R. Ahuja, H. Arwin, A. Ferreira da Silva, C. Persson, J.M. Osorio-Guille'n, J. Souza de Almeida, C. Moyses Araujo, E. Veje, N. Veissid, C.Y. An, I. Pepe, B. Johansson, Electronic and optical properties of lead iodide, *J. Appl. Phys.* 92 (2002) 7219.
- [42] M. Baibarac, N. Preda, L. Mihut, I. Baltog, S. Lefrant, J.Y. Mevellec, On the optical properties of micro- and nanometric size Pbl<sub>2</sub> particles, *J. Phys. Condens. Matter.* 16 (2004) 2345.
- [43] N. Preda, L. Mihut, M. Baibarac, I. Baltog, S. Lefrant, A distinctive signature in the Raman and photoluminescence spectra of intercalated Pbl<sub>2</sub>, *J. Phys. Condens. Matter.* 18 (2006) 8899.
- [44] I. Baltog, S. Lefrant, L. Mihut, R.P. Mondescua, Luminescence of Pbl<sub>2</sub> Cu<sup>+</sup> 63 (1995) 309.
- [45] M. Matuchova, K. Zdansky, J. Zavadil, A. Danilevsky, J. Maixner, D. Alexiev, Electrical, optical and structural properties of lead iodide, *J. Mater. Sci. Mater. Electron.* 20 (2008) 289.
- [46] W.W. Gärtner, Depletion-layer photoeffects in semiconductors, *Phys. Rev.* 116 (1959) 84.
- [47] J. Li, R. Peat, L.M. Peter, J. Li, R. Peat, Surface recombination at semiconductor electrodes, *J. Electroanal. Chem. Interfacial Electrochem.* 165 (1984) 41.
- [48] D. Vanmaekelbergh, B.H. Erne, C.W. Cheung, R.W. Tjerkstra, On the increase of the photocurrent quantum efficiency of GaP photoanodes due to (photo) anodic pretreatments, *Electrochim. Acta.* 40 (1995) 689.
- [49] D.J. Fermin, E.A. Ponomarev, L.M. Peter, Kinetic study of CdS photocorrosion by intensity modulated photocurrent and photoelectrochemical impedance spectroscopy, *J. Electroanal. Chem.* 473 (1999) 192.
- [50] A. Manchon, H.C. Koo, J. Nitta, S.M. Frolov, R.A. Duine, New perspectives for Rashba spin-orbit coupling, *Nat. Mater.* 14 (2015) 871.
- [51] D. Niesner, M. Wilhelm, I. Levchuk, A. Osvet, S. Shrestha, M. Batentschuk, C. Brabec, T. Fauster, Giant Rashba Splitting in CH<sub>3</sub>NH<sub>3</sub>PbBr<sub>3</sub> Organic-Inorganic Perovskite, *Phys. Rev. Lett.* 117 (2016) 126401.
- [52] T. Etienne, E. Mosconi, F. De Angelis, Dynamical Origin of the Rashba Effect in Organohalide Lead Perovskites: A Key to Suppressed Carrier Recombination in Perovskite Solar Cells? *J. Phys. Chem. Lett.* 7 (2016) 1638.